Immunity
Article

Structure of Myxovirus Resistance Protein A Reveals Intra- and Intermolecular Domain Interactions Required for the Antiviral Function

Song Gao,[1,2,6,*] Alexander von der Malsburg,[3,6] Alexej Dick,[1] Katja Faelber,[1] Gunnar F. Schröder,[4] Otto Haller,[3] Georg Kochs,[3] and Oliver Daumke[1,5,*]
[1]Max-Delbrück-Centrum for Molecular Medicine, Crystallography, Robert-Rössle-Strasse 10, 13125 Berlin, Germany
[2]Institute for Chemistry and Biochemistry, Freie Universität Berlin, Takustrasse 3, 14195 Berlin, Germany
[3]Department of Virology, Institute for Medical Microbiology and Hygiene, University of Freiburg, Hermann-Herder-Strasse 11, 79104 Freiburg, Germany
[4]Institute of Complex Systems (ICS-6), Forschungszentrum Jülich, Wilhelm-Johnen-Strasse, 52425 Jülich, Germany
[5]Institute of Medical Physics and Biophysics, Charité, Ziegelstrasse 5-9, 10117 Berlin, Germany
[6]These authors contributed equally to this work
*Correspondence: song.gao@mdc-berlin.de (S.G.), oliver.daumke@mdc-berlin.de (O.D.)
DOI 10.1016/j.immuni.2011.07.012

SUMMARY

Human myxovirus resistance protein 1 (MxA) is an interferon-induced dynamin-like GTPase that acts as a cell-autonomous host restriction factor against many viral pathogens including influenza viruses. To study the molecular principles of its antiviral activity, we determined the crystal structure of nucleotide-free MxA, which showed an extended three-domain architecture. The central bundle signaling element (BSE) connected the amino-terminal GTPase domain with the stalk via two hinge regions. MxA oligomerized in the crystal via the stalk and the BSE, which in turn interacted with the stalk of the neighboring monomer. We demonstrated that the intra- and intermolecular domain interplay between the BSE and stalk was essential for oligomerization and the antiviral function of MxA. Based on these results, we propose a structural model for the mechano-chemical coupling in ring-like MxA oligomers as the principle mechanism for this unique antiviral effector protein.

INTRODUCTION

Innate immunity plays an important role in early host defense against invading viruses. Intracellular restriction factors can severely limit transspecies transmission and spread of viral pathogens, as best illustrated in the case of zoonotic transmissions of primate lentiviruses (reviewed in Wolf and Goff, 2008). In mammals and other vertebrates, the interferon (IFN)-induced myxovirus resistance (Mx) proteins are powerful antiviral factors restricting a broad range of viruses, including influenza viruses (Haller and Kochs, 2011). Recent evidence suggests that the human MxA protein most probably provides a barrier against zoonotic introduction of influenza A viruses into the human population (Zimmermann et al., 2011).

The critical role of Mx proteins in antiviral protection has previously been established in cell culture and animal model systems, foremost the mouse. In contrast to wild-type mice and rare inbred strains derived from them, most laboratory strains carry deletions or nonsense mutations in the *Mx1* gene and, consequently, are highly susceptible to infection with pathogenic influenza and influenza-like viruses (Staeheli et al., 1988). Mx gene expression depends on induction by type I (alpha or beta) or type III (lambda) IFNs (Holzinger et al., 2007), whereas the action of Mx proteins is IFN independent. Thus, constitutive expression of recombinant mouse or human Mx proteins protects transgenic laboratory mice against infection with Mx-sensitive viruses even in the absence of an IFN response (Staeheli et al., 1986). A direct role of Mx proteins was demonstrated by the fact that the Mx antiviral activity can be neutralized in living cells by microinjection of specific antibodies (Arnheiter and Haller, 1988). Besides its antiviral function, MxA expression has also been linked to increased sensitivity of cells to apoptotic stimuli (Mibayashi et al., 2002) and to inhibition of tumor cell motility and invasiveness (Mushinski et al., 2009). Moreover, the mouse Mx1 protein has been characterized as one of the few minor histocompatibility antigens (Speiser et al., 1990).

Mx proteins are large GTPases and belong to a group of IFN-induced GTPases involved in the control of intracellular pathogens. These include the immunity-related p47 GTPases and the guanylate-binding proteins (GBPs or p65 GTPases) known to restrict the growth of invading bacteria and protozoa (Hunn et al., 2011). Given their sequence similarity and biochemical and structural properties, Mx proteins strongly resemble the class of dynamin-like GTPases that mediate basic cellular processes involving membrane remodeling (Low and Löwe, 2010; Haller and Kochs, 2011). Also, the human MxA GTPase is closely associated with intracellular membranes, preferentially of the endoplasmic reticulum-Golgi intermediate compartment (Accola et al., 2002; Stertz et al., 2006), which is abused by

Table 1. Crystallographic Data Collection and Refinement Statistics

	MxA[a]	MxA$^{\Delta 1\text{-}32a}$	SeMet MxA[a]
Data Collection			
Space group	C2	C2	C2
Cell dimensions			
a, *b*, *c* (Å)	146.9, 137.6, 57.7	156.8, 134.0, 58.1	150.5, 138.1, 57.6
α, β, γ (°)	90.0, 106.9, 90.0	90.0, 106.3, 90.0	90.0, 106.5, 90.0
Beamline	BESSY MX14.1	BESSY MX14.1	SLS X06SA
Wavelength (Å)	0.91841	0.91841	0.97960
Total reflections[b]	22,042 (3,152)	31,669 (5,141)	24,155 (1,819)
Unique reflections[b]	7,012 (1,076)	10,349 (1,699)	6,816 (532)
Resolution (Å)[b]	31–3.50 (4.41–3.50)[c]	100–3.50 (4.15–3.50)[d]	50–5.60 (5.75–5.60)
R_{sym}[b]	0.064 (0.341)	0.097 (0.595)	0.077 (0.712)
$I/\sigma I$[b]	12.38 (4.30)	9.33 (2.25)	8.76 (2.01)
Completeness (%)[b]	50.3 (15.5)	70.6 (29.0)	98.8 (96.6)
Redundancy	3.14 (2.93)	3.06 (3.03)	3.54 (3.42)
Refinement			
Resolution (Å)	31–3.5	35–3.5	
R_{work}	0.306	0.262	
R_{free}	0.333	0.295	
Number of atoms			
Protein	4,642	4,507	
Water	0	0	
Rms deviations			
Bond lengths (Å)	0.006	0.015	
Bond angles (°)	0.931	1.583	

[a] MxA refers to the human MxA protein containing the quadruple point mutation YRGR440-443AAAA and deletion of amino acid residues 533–561. Because of the better quality, the MxA$^{\Delta 1\text{-}32}$ data were used for final refinement.
[b] Numbers in parentheses represent values from the highest resolution shell.
[c] Resolution limits along a*, b*, and c* are 4.5 Å, 5.5 Å, and 3.5 Å, respectively.
[d] Resolution limits along a*, b*, and c* are 4.0 Å, 4.2 Å, and 3.5 Å, respectively.

many viral pathogens as an intracellular replication site (Miller and Krijnse-Locker, 2008).

Like most dynamin-like GTPases, Mx proteins are composed of an amino-terminal (N-terminal) GTPase (G) domain, a central middle domain (MD), and a carboxy-terminal (C-terminal) GTPase effector domain (GED). Similarly to dynamin, human MxA assembles into tetramers and shows low-affinity binding of guanine nucleotides, concentration-dependent oligomerization, and assembly-stimulated GTPase activation (Gao et al., 2010). We previously determined the structure of the stalk of MxA, which folds into a four-helical bundle composed of the MD and the N-terminal part of the GED (Gao et al., 2010). This stalk was found to mediate the assembly of MxA into tetramers and higher-order oligomers via three distinct interfaces and two loop regions. Based on the similar appearance of MxA and dynamin oligomers in electron microscopy images (Mears et al., 2007; von der Malsburg et al., 2011) and based on the almost identical localization of amino acid residues dictating oligomerization of the stalks (Ramachandran et al., 2007; Gao et al., 2010), we suggested that the overall architecture of the MxA and dynamin oligomers is largely the same. To understand the molecular basis of its antiviral function, we here describe the structure of full-length MxA and determine the role of the structural elements for oligomerization, GTP hydrolysis, and antiviral activity.

RESULTS

Structure of the Full-Length MxA Monomer

Crystallization trials with full-length wild-type (WT) MxA did not yield protein crystals. With electron microscopy, we previously observed that WT MxA can reversibly assemble into regular, filamentous, and ring-shaped, higher-order oligomers that can be sedimented by ultracentrifugation (Kochs et al., 2002a). Mutations in the three assembly interfaces in the stalk, however, prevent formation of sedimentable oligomers and, concurrently, interfere with the antiviral activity (Gao et al., 2010). We reasoned that the higher-order oligomers formed by WT MxA might not be compatible with crystal formation and therefore assayed assembly-defective stalk mutants for crystallization. Indeed, crystals of an MxA variant carrying four amino acid exchanges in interface-3 (YRGR440-443AAAA) and a deletion of 29 amino acids in the predicted substrate binding loop L4^{S} (533-561) (ΔL4^{S}) were obtained, which anisotropically diffracted to a maximum resolution of 3.5 Å (Table 1). The structure was solved by

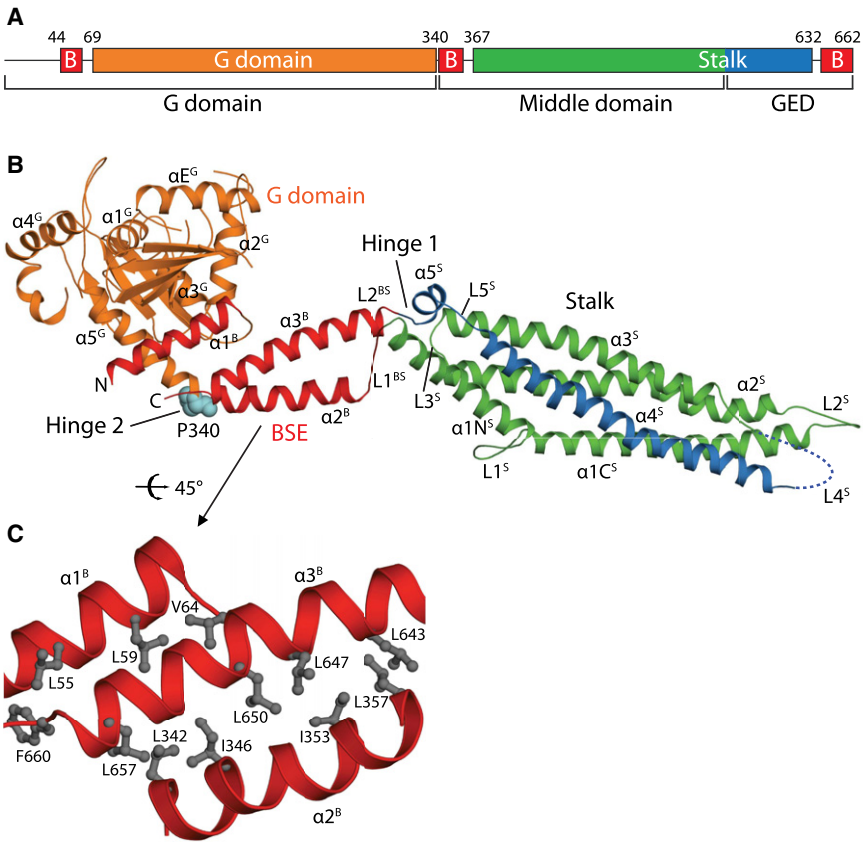

Figure 1. Structure of the MxA Monomer

(A) Structure-based domain representation of human MxA. B, BSE. The previous terminology based on sequence alignments is indicated below.

(B) Ribbon-type representation of an MxA monomer, colored as in (A), with individual domains and the two hinges specified. N and C termini as well as secondary structure elements are labeled. The unresolved truncated loop $L4^S$ in the stalk is indicated by a dashed line. The invariant Pro340 linking G domain and BSE (hinge 2) is shown as spheres in cyan.

(C) Structural details of the BSE. The three-helical bundle is shown in ribbon-type representation and residues of the hydrophobic core of the BSE are shown in ball-and-stick representation. G domain and $L1^{BS}$ were removed for clarity.

See also Figure S1 and Table 1.

molecular replacement with the structure of the MxA stalk (Gao et al., 2010) and the nucleotide-free G domain of dynamin (Reubold et al., 2005) as search models, and refined to an R_{work} of 26.2% and an R_{free} of 29.5% (Table 1). To verify the sequence assignment, the positions of nine methionines were determined by calculating an anomalous difference Fourier map from selenomethione (SeMet)-substituted MxA crystals (see Figure S1A available online). Even at this moderate resolution, side chain density for a number of residues also in previously undefined regions became apparent (Figures S1B–S1D). The model begins at Tyr45 and ends at the final C-terminal residue of MxA, Gly662, with four gaps in the G domain and one in the truncated loop $L4^S$ in the stalk.

MxA appeared as an elongated molecule with a three-domain architecture composed of the G domain, the bundle signaling element (BSE), and the stalk (Figures 1A and 1B). Some parts of the globular G domain were only weakly defined in the electron density. It consisted of a central β sheet surrounded by α helices (Figure 1B). The two switch regions known to mediate nucleotide-dependent changes were not visible in the electron density. Also, the G4 and the *cis*- and *trans*-stabilizing loops, contributing to dimerization of G domains in dynamin (Chappie et al., 2010), were mostly invisible. The stalk was located at the opposing end of the MxA molecule. It was built of an extended four-helical bundle ($\alpha1^S$–$\alpha4^S$, where superscripts G, B, and S stand for G domain, BSE, and stalk, respectively) and had an almost identical architecture to the isolated stalk of MxA (Figure 1B; Gao et al., 2010). However, loop $L2^S$, which is not visible in the free stalk structure, was fully resolved. It contained the YRGR440-443AAAA mutation required for crystallization.

Strikingly, the BSE formed an extended structure in the center of the MxA molecule (Figure 1B). It was composed of three helices ($\alpha1^B$–$\alpha3^B$), which were derived from widely dispersed sequence regions of MxA and, consequently, were not coinciding with the domain boundaries delineated from the primary sequence (Figure 1A). $\alpha2^B$ and $\alpha3^B$ formed a profound hydrophobic network (Figures 1C and S1E), whereas $\alpha1^B$ was only weakly associated with $\alpha2^B$ and $\alpha3^B$ via a few hydrophobic interactions (Figures 1C and S1F). Interestingly, Glu645 in $\alpha3^B$, whose mutation to arginine alters the antiviral specificity of MxA (Zürcher et al., 1992a; Kochs et al., 2002b), was accessible to the solvent (Figure S1G). The overall architecture of this domain was very similar to the BSE of dynamin (Chappie et al., 2009, 2010).

At the N terminus, the G domain was connected to helix $\alpha1^B$ of the BSE and at the C terminus to $\alpha2^B$ via the invariant Pro340 (Figure 1B). Corresponding prolines in dynamin (Chappie et al., 2010), bacterial dynamin-like protein (BDLP) (Low and Löwe, 2010), GBP1 (Prakash et al., 2000), atlastin1 (Byrnes and Sondermann, 2011; Bian et al., 2011), and Eps15 homology-domain containing protein 2 (EHD2) (Daumke et al., 2007) have previously been suggested to act as a hinge (hinge 2 according to Low and Löwe [2010]) to mediate conformational coupling of G domain and stalk (Figures 2 and S2). Our structure revealed that the BSE was connected to the stalk via an additional hinge (hinge 1) composed of loop $L1^{BS}$ and $L2^{BS}$ (Figures 1B and 3A). $L1^{BS}$ was in a stretched conformation and interacted loosely with $L2^{BS}$ and $\alpha5^S$ of the stalk (Figures 3A and S3A). Additionally, the highly conserved Arg640 of $\alpha3^B$ formed polar contacts with Gly361 and Asp363 of $L1^{BS}$ and the invariant Glu632 in the center of $L2^{BS}$ (Figures 3A and S3B). Hinge 1 was previously described in BDLP, but not in GBP1, EHD2, and atlastin that do not have a BSE-like structural element (Figure 2). Interestingly, a mutation of Arg725 in the homologous hinge 1 of dynamin corresponding

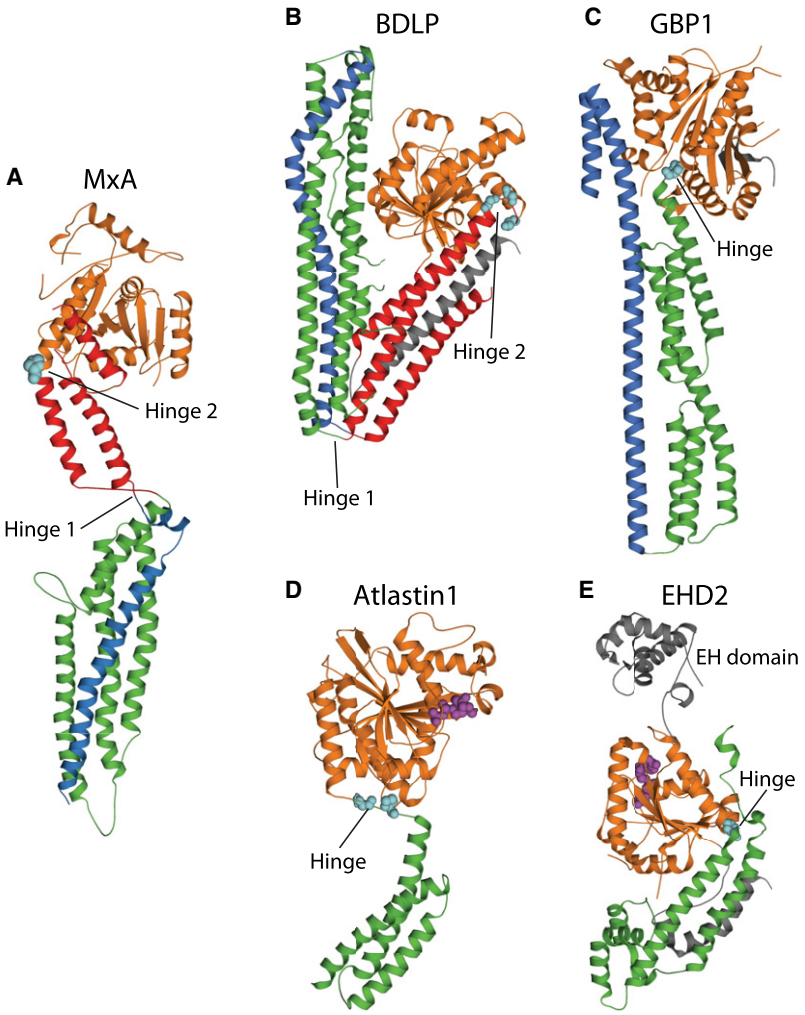

Figure 2. Structural Comparison of MxA with Other Dynamin Superfamily Members

Structural comparison of MxA (A) with nucleotide-free BDLP (PDB accession code 2J69) (B), nucleotide-free GBP1 (1DG3) (C), GDP-bound atlastin1 (3Q5D) (D), and EHD2 in the presence of a nonhydrolyzable ATP analog (2QPT) (E). G domains are colored in orange, stalk-like structures in green (derived from the middle domain) and blue (derived from the GED), and the BSE in red. Prolines in the hinge regions are shown as cyan spheres, and nucleotides are shown in purple. A separate BSE is apparent only in MxA and BDLP, whereas a proline residue-containing hinge region is found in all structures. See also Figure S2.

to Arg640 in MxA leads to reduced GTPase activity upon microtubule association but increased endocytosis efficiency (Sever et al., 1999), suggesting that stabilization of hinge 1 contributes to the conformational coupling of the G domain and the stalk. Furthermore, a mutation in hinge 1 of rat Mx2 was shown to abolish the antiviral activity (Figure S3C; Johannes et al., 1997).

Hinge 1 Controls Oligomerization and the Antiviral Activity of MxA

To investigate the function of hinge 1, oligomerization assays were carried out. At protein concentrations >2 mg/ml, MxA reversibly forms higher-order oligomers that can be sedimented by ultracentrifugation (Gao et al., 2010). Guanine nucleotides promote oligomerization, most probably by creating an additional nucleotide-dependent interface in the G domain, as suggested for dynamin (Chappie et al., 2010). Accordingly, 50% of WT MxA oligomerized in the absence of nucleotide, whereas more than 90% was sedimented in the presence of a nonhydrolyzable GTP analog, guanosine 5′-O-[gamma-thio]triphosphate (GTPγS) (Figure 3B). Two mutants in hinge 1, E632A in $L2^{BS}$ and R640A in $\alpha3^{B}$, did not oligomerize in the absence of nucleotides. However, in the presence of GTPγS, E632A still oligomerized to some degree whereas the R640A mutant was completely in the supernatant (Figure 3B). These data were further corroborated by gel filtration and right angle light scattering (RALS) analysis (Figure S3D), where WT MxA, in the absence of nucleotide, showed a dimer-tetramer equilibrium and mutants E632A and R640A were mostly dimeric (Figure S3D), indicating that an intact hinge 1 is important for the native assembly of MxA oligomers.

Our previous analysis of stalk mutants indicated that higher-order oligomerization of MxA reduces the off-rate for GTP, which might become rate-limiting in GTPase reactions at high protein concentrations (Gao et al., 2010). To test whether oligomerization mediated by the hinge 1 region is also involved in this regulation, GTPase activities of the hinge mutants were monitored at different protein concentrations via multiple-turnover assays at saturating GTP concentrations. WT MxA showed a cooperative GTPase reaction with an estimated k_{max} of 6 min^{-1} (Figure 3C). The E632A mutant displayed a 5-fold increase in maximal GTPase activity, whereas the R640A mutation in the center of hinge 1 led to a dramatically accelerated GTP turnover already at low protein concentrations. Thus, an intact hinge 1 was required for higher-order oligomerization of MxA and efficient control of the GTPase activity in solution, which might avoid futile cycles of GTP hydrolysis in its ground state.

To investigate the role of hinge 1 for the antiviral activity of MxA, the E632A and R640A mutants were tested in a La Crosse Virus (LACV) infection assay (Kochs et al., 2002b; Reichelt et al., 2004). As previously described, when WT MxA-expressing cells were infected, the nucleoprotein N of LACV was sequestered into perinuclear structures. Formation of these MxA-N aggregates is considered to be the basis of the antiviral effect of MxA against LACV (Reichelt et al., 2004). An assembly-defective mutant carrying a deletion of the putative substrate binding loop L4 MxA ($\Delta L4^{S}$) (von der Malsburg et al., 2011) was used as a negative control and showed no redistribution (Figure 3D; Gao et al., 2010). The E632A mutant in hinge 1 still relocalized to granular structures and colocalized with LACV nucleoprotein (Figure 3D). This finding might be explained by the fact that this mutant was still able to form oligomers in the presence of

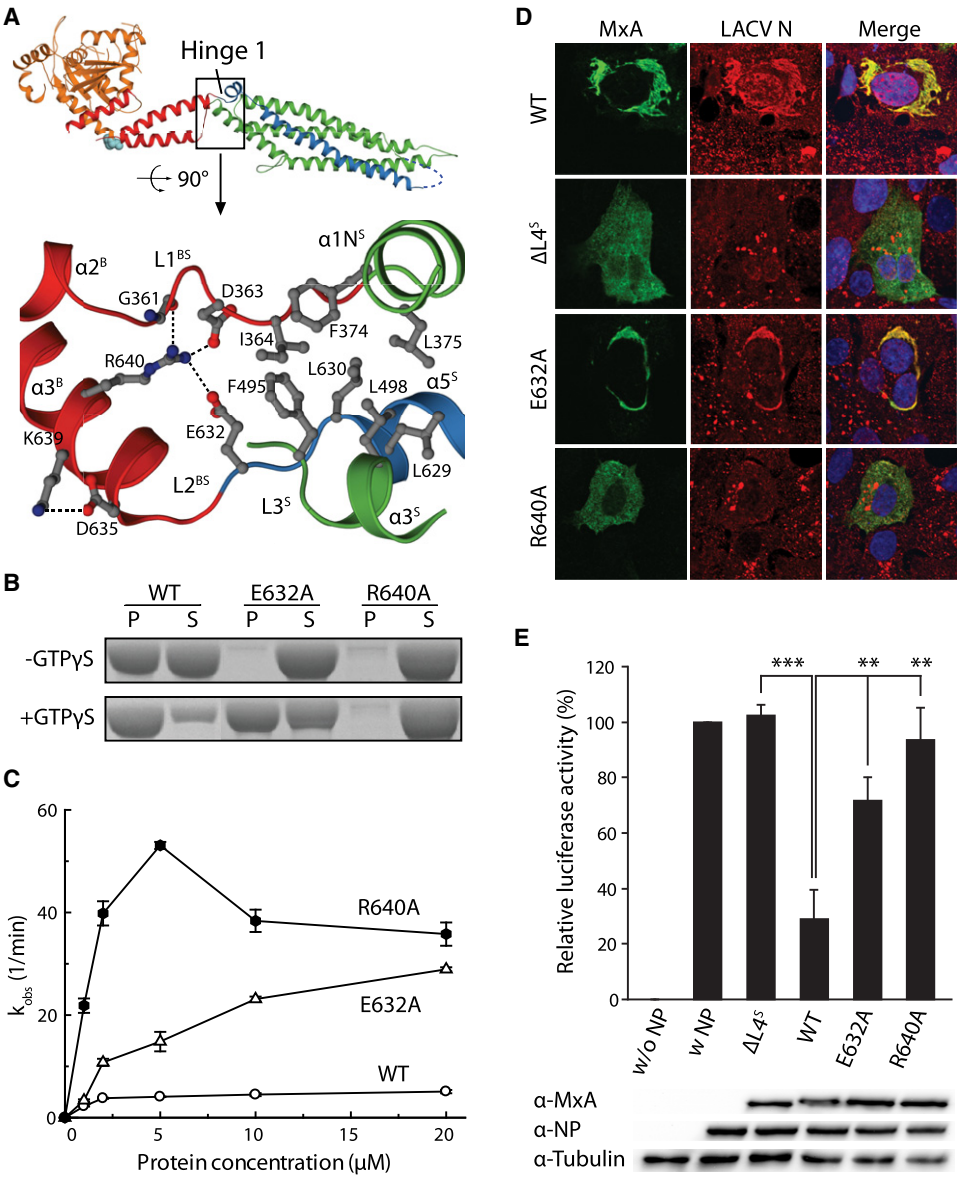

Figure 3. Integrity of Hinge 1 Is Important for the Function of MxA

(A) Structure of hinge 1 connecting BSE and stalk, with selected residues shown in ball-and-stick representation.

(B) Sedimentation experiments for WT MxA and selected mutants in hinge 1 were carried out in the absence and presence of 1 mM GTPγS. P, pellet fraction; S, supernatant.

(C) Protein-concentration-dependent GTPase activities with excess of GTP over protein of WT MxA (open circle) and hinge 1 mutants E632A (open triangle) and R640A (closed circle) were determined at 150 mM NaCl. The mean of k_{obs} calculated from two independent experiments is indicated with the error bars showing the range of the two data points.

(D) Complex formation of MxA with the LACV nucleoprotein (N). Vero cells transfected with the indicated MxA constructs were infected with LACV for 16 hr and then stained with antibodies specific for MxA (green) and LACV N (red). In the overlays, a nuclear staining via TO-PRO dye is shown in blue. A total of 99% of the cells transfected with WT MxA contained MxA-N complexes, compared to 97% for E632A. No complex formation (0%) was observed for R640A (n = 100). The $\Delta L4^S$ mutant is shown as a negative control (Gao et al., 2010).

(E) Minireplicon assay for influenza A virus polymerase. 293T cells were transfected with plasmids encoding viral nucleoprotein (NP), the polymerase subunits, and a reporter construct encoding firefly luciferase under the control of the viral promoter. Expression plasmids for the indicated MxA constructs and for Renilla luciferase under a constitutive promoter were cotransfected. Twenty-four hours later, the activity of firefly luciferase was measured and normalized to the activity of Renilla luciferase. The values without MxA expression were set to 100%. Error bars and standard deviations are indicated (n = 3). Protein expression was analyzed by immunoblotting with specific antibodies. Significance was calculated with Student's t test (n = 3). n.s., not significant; $^{**}p \leq 0.01$; $^{***}p \leq 0.001$.

See also Figure S3.

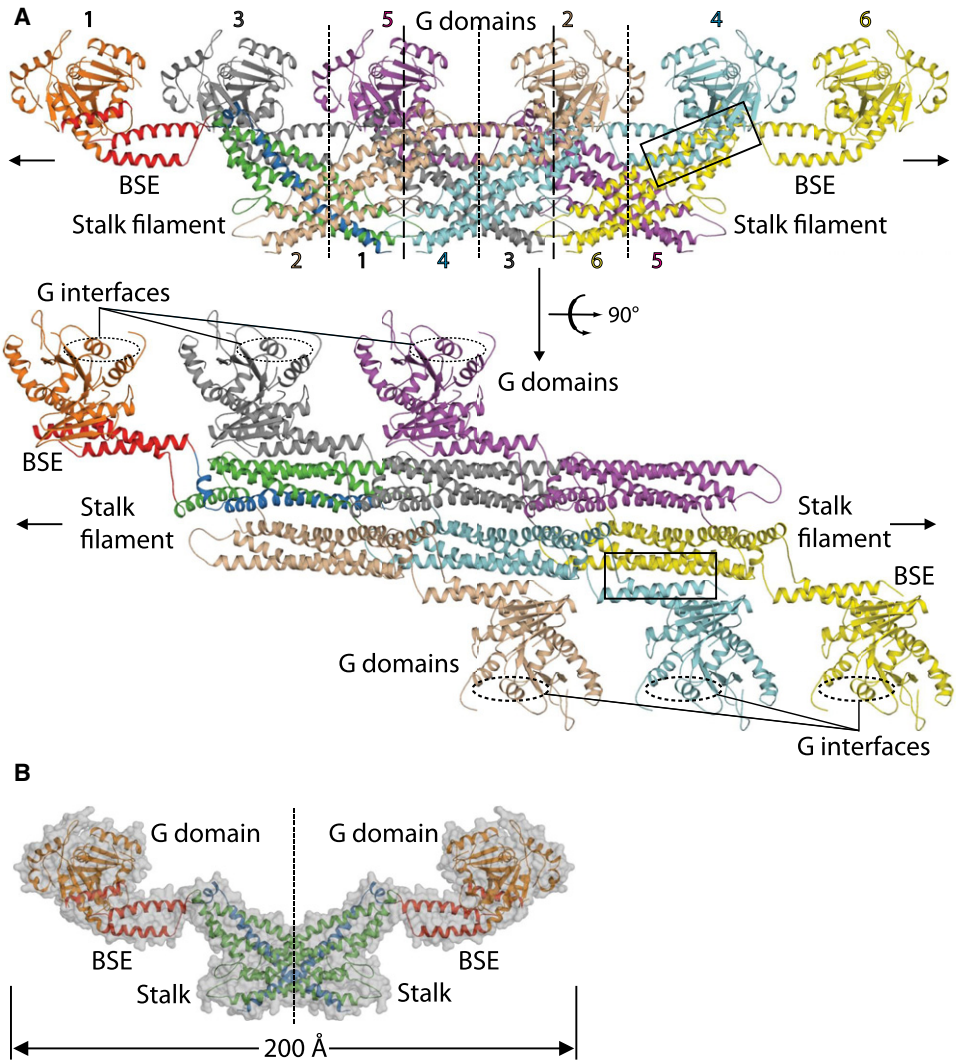

Figure 4. Structure of the MxA Oligomer

(A) Two views of the MxA oligomer represented by six MxA monomers, as seen in the crystals. Monomer 1 is colored as in Figure 1B. The interaction site of the BSE in monomer 4 with the neighboring stalk of monomer 6 is indicated by a black box. In the upper panel, crystallographic 2-fold axes are indicated by dashed lines. In the lower panel, putative G domain-G domain dimerization sites (G interfaces) are specified.

(B) Ribbon-type representation of the MxA dimer with a transparent surface, spanning 200 Å. The crystallographic 2-fold axis across interface-2 is indicated by a dashed line.

See also Figure S4.

nucleotide (Figure 3B). However, replacement of the central Arg640 by an alanine led to a diffuse distribution of the protein within the cell and the R640A mutant failed to sequester the viral nucleoprotein (Figure 3D), highlighting the importance of hinge region 1 for the antiviral activity.

MxA has been described as the key interferon-induced effector protein against influenza A viruses that blocks an early step of the viral replication (Pavlovic et al., 1992). To evaluate the role of hinge 1 for the inhibition of viral gene expression, a minireplicon reporter assay using the polymerase of a highly pathogenic H5N1 influenza virus was performed (Gao et al., 2010). In these experiments, WT MxA inhibited viral RNA polymerase by >70% whereas the MxA (ΔL4^S) mutant was inactive (Figure 3E). Mutations in hinge 1 completely abolished (R640A) or reduced (E632A) the inhibitory effect of MxA. Collectively, these results showed that an intact hinge 1 was essential for the antiviral function of MxA.

Self-Assembly of MxA and Its Importance for Antiviral Activity

MxA monomers in the crystals assembled via the stalks in a criss-cross pattern to form a linear stalk filament (Figure 4A; Figure S4A). This arrangement via three distinct interfaces was almost identical to the previously reported assembly of the isolated MxA stalks (rmsd of 0.6 Å for the C_α atoms of the stalk dimers) (Gao et al., 2010). The symmetric interface-2 in the center of the stalks mediated dimerization of MxA (Figure 4B), whereas interface-1 and interface-3 facilitated contacts between

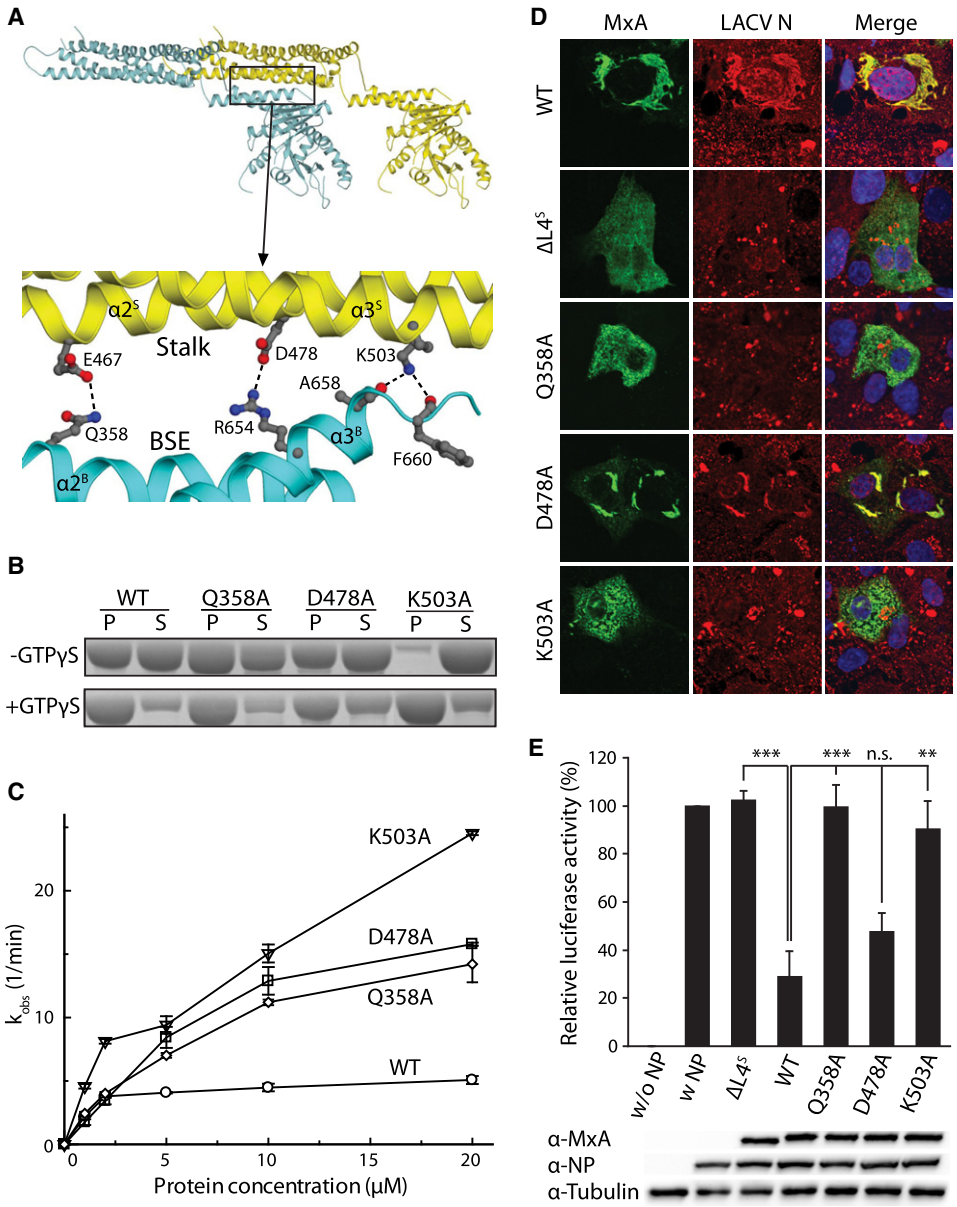

Figure 5. BSE-Stalk Interactions Mediate Oligomerization and Antiviral Activity

(A) Intermolecular interactions between BSE and stalk of two parallel monomers (e.g., monomer 4 and 6 from Figure 4A). Residues involved in this interface are shown in ball-and-stick representation.

(B) Sedimentation experiments for WT MxA and the indicated mutants were carried out as described in Figure 3B.

(C) Protein-concentration-dependent GTPase activities were determined as described in Figure 3C, with WT MxA (open circles) and the Q358A (open diamond), D478A (open circle), and K503A (open triangle) point mutants.

(D) Complex formation of WT MxA and the indicated mutants with the LACV nucleoprotein was determined as described in Figure 3D. A total of 99% of the cells transfected with WT MxA contained MxA-N complexes, compared to 94% for D478A. No complex formation (0%) was observed for Q358A and K503A (n = 100). The $\Delta L4^S$ mutant is shown as a negative control.

(E) Minireplicon assay for influenza A virus polymerase for WT MxA and the indicated mutants as described in Figure 3E.

See also Figure S5.

MxA dimers and allowed the formation of stable tetramers as well as higher-order oligomers (Figures S4B–S4D). In the full-length structure, loop $L2^S$ was now identified as a structural component of interface-3. It interacted with helix $\alpha4^S$ and possibly $L4^S$ of the stalk of an opposite, antiparallel MxA monomer (Figure S4D), which might explain its role in stabilization of the MxA oligomer (Gao et al., 2010). Interestingly, $\alpha2^B$ of the BSE contacted the stalk of a neighboring parallel MxA monomer via a number of polar interactions (Figures 4A, 5A, and S5A). In particular, Glu467 and Asp478 in $\alpha2^S$ interacted with Gln358 in $\alpha2^B$ and Arg654 in $\alpha3^B$, respectively, whereas Lys503 in $\alpha3^S$ formed hydrogen bonds with the peptide backbone of $\alpha3^B$. In

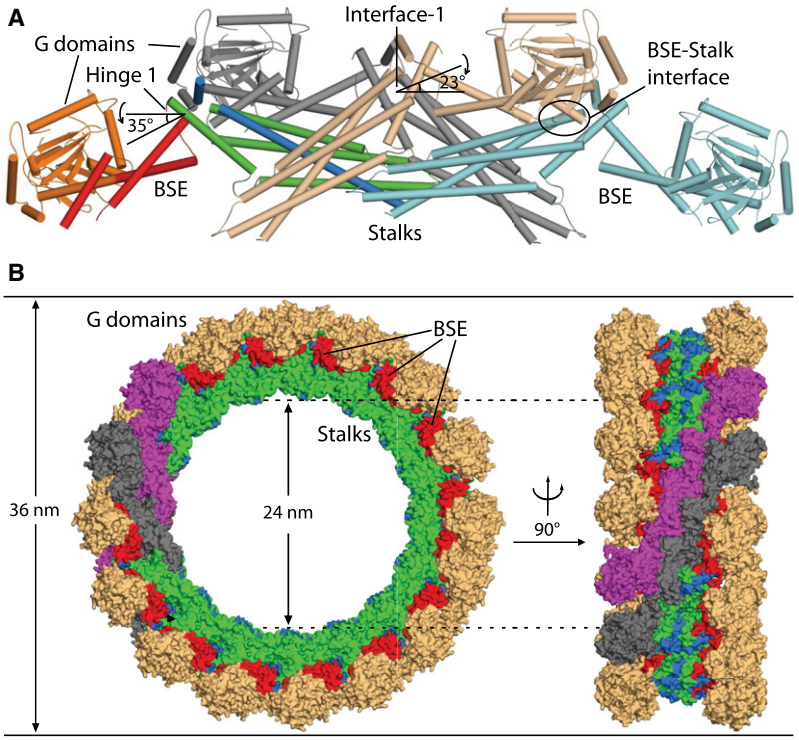

Figure 6. Model of Ring-like MxA Oligomer Suggests a Mechanism for the Mechano-Chemical Coupling

(A) Construction of ring-like MxA oligomers, as indicated for an MxA tetramer. The indicated 23° rotation around the flat hydrophobic interface-1 leads to the formation of ring-like MxA oligomers. The BSE-stalk interface via Lys503 is maintained by a 35° rotation of the G domain and BSE versus the stalk around hinge 1. This tetramer was used to construct a model for a ring-like MxA oligomer.

(B) Model of ring-like MxA oligomer shown as space-filling representation. The individual domains are colored as in Figure 1A, except for the G domains, which are colored in light orange. Two MxA dimers are individually highlighted in magenta and gray. The MxA ring is composed of 16 constitutive dimers.

See also Figure S6 and Movie S1.

the stalk filament, this interaction took place at the opposite side compared to the central stalk-stalk interaction sites (Figure 4A).

In oligomerization assays, the Q358A and D478A mutants in the BSE-stalk interface behaved similar to WT MxA (Figure 5B). However, gel filtration combined with right angle light scattering analysis showed that the Q358A mutant eluted preferentially as dimer, whereas the D478A mutant behaved like wild-type MxA (Figure S5B), indicating a minor contribution of D478A to the stability of the oligomer. Strikingly, the K503A mutant in $\alpha 3^S$ did not oligomerize in the absence of nucleotides, but addition of GTPγS rescued oligomerization (Figures 5B and S5B). These data indicated that the MxA oligomer was stabilized not only by stalk-stalk interactions, but additionally via contacts between the stalk and the BSE of neighboring molecule.

In protein-concentration-dependent GTPase assays, the Q358A and D478A mutants in the BSE-stalk interface showed a 2- to 3-fold increased activity at higher protein concentrations when compared to the wild-type, whereas the K503A mutant had an even 5-fold increased GTPase rate (Figure 5C), confirming the central function of Lys503 in this BSE-stalk interface. We recently showed that mutations interfering with tetramerization of MxA display increased GTPase rates, possibly by overcoming mobility restrictions in the rigid structure of the MxA tetramer (Gao et al., 2010). Increased flexibility of the G domains might then promote G domain dimerization in solution, leading to increased GTPase rates. Consequently, our data indicated an auto-inhibitory function of the BSE-stalk interface for the GTPase activity of MxA.

In antiviral activity assays against LACV, both the Q358A and the K503A mutants in the BSE-stalk interface showed a diffuse cellular distribution, comparable to MxA($\Delta L4^S$), suggesting a requirement of the BSE-mediated stalk interactions for the antiviral activity. In agreement with our oligomerization and RALS data, mutant D478A was still capable of associating with LACV nucleoprotein (Figure 5D). Likewise, the D478A mutant was still active in the influenza minireplicon assay, whereas the Q358A and K503A mutants lost their antiviral function (Figure 5E). These results indicated a central function of residue Lys503 and, additionally, Gln358 for the BSE-stalk interaction and a critical role of this interface for the antiviral activity of the MxA oligomer.

Structural Model of MxA Oligomeric Rings

In the crystals, the linear MxA filaments assembled via the stalks, but the G domains did not dimerize via the highly conserved interface across the nucleotide binding site (Figure S6; Chappie et al., 2010). In contrast to these linear oligomers, ring-like MxA oligomers were observed around tubulated liposomes in electron microscopy studies (Accola et al., 2002; von der Malsburg et al., 2011). We previously suggested that flat hydrophobic interface-1 allows rotation of dimeric MxA stalks assembled via interface-2 (Figure 6A; Movie S1). By using this rotation and our full-length MxA structure, we constructed ring-like MxA oligomers with a diameter as described in the electron microscopy studies (Figure 6B). The BSE was slightly adjusted to allow Lys503 contact the stalk. Compared to our previous model (Gao et al., 2010), the G domains were located above the stalk not of the same but of the neighboring molecule. This difference originated from the introduction of the elongated BSE in our current model whose structure was previously unknown. In the resulting model of the MxA rings (Figure 6B), the stalks were forming the inner layer and G domains the outer layer of the oligomer. The predicted substrate binding loop $L4^S$ pointed toward the inside of the ring and could interact with viral or membranous target structures. Most importantly, conformational changes of the G domain could be transmitted to the stalk via the identified BSE-stalk interface.

DISCUSSION

Since the discovery of Mx resistance against influenza viruses in mice (Lindenmann, 1964) and the cloning of the Mx gene

(Staeheli et al., 1986), much effort has been devoted to explore the antiviral mechanism of Mx proteins (Haller and Kochs, 2011). The antiviral activity of MxA was shown to be dependent on two essential features, namely GTP hydrolysis performed by the G domain (Pitossi et al., 1993) and oligomerization mediated by the MD and GED (Melén et al., 1992; Schwemmle et al., 1995; Di Paolo et al., 1999; Gao et al., 2010). We recently demonstrated that the MD and the N-terminal portion of the GED together form a separate domain, the stalk of MxA, and elucidated the molecular basis of oligomerization via this domain (Gao et al., 2010). Interestingly, mutations or deletions in the MD and/or GED were shown to influence GTPase activity (Schwemmle et al., 1995; Gao et al., 2010), suggesting that a modular cross-talk between G domain and stalk is required for antiviral effector functions. However, because of the lack of structural data for full-length Mx and/or the related dynamin proteins, the molecular basis of this cross-talk has remained elusive.

In our full-length MxA structure, we identified the BSE as the third domain of MxA and demonstrated that it served an important function in mediating oligomerization, as suggested by previous biochemical studies (Di Paolo et al., 1999). The unique architecture of the BSE involving elements from three widely separated regions and its central localization in the MxA molecule suggested a crucial role as transmitter of conformational changes between the G domain and stalk. The two hinge regions flanking the BSE appeared to be flexible and might allow interdomain movements. Interestingly, some stability of hinge 1 was essential for the assembly of the MxA oligomer, as demonstrated by our mutagenesis studies. The extended shape of the full-length MxA dimer (Figure 4B) resembled a low-resolution envelope of a dimeric dynamin variant obtained by small angle X-ray scattering (Kenniston and Lemmon, 2010), indicating a similar architecture and mechanism.

How are domain movements in MxA initiated? For BDLP, large-scale domain movements of the G domain versus the stalk are triggered by GTP-dependent oligomerization on a lipid template (Low and Löwe, 2010). This process involves dimerization of G domains via an interface across the nucleotide binding site (the G interface). Also in dynamin, nucleotide-dependent dimerization of G domains via the G interface leads to stimulation of the GTPase reaction (Chappie et al., 2010). The G interface is highly conserved in the dynamin family, suggesting a similar mechanism also for MxA (Figure 4A). However, in the linear MxA filaments in our crystals, G domains of neighboring filaments did not dimerize via the G interface. This implies that the current nucleotide-free structure represents a functional state of the MxA oligomer in which oligomerization is solely mediated by stalk-stalk and BSE-stalk interactions. We envisage that nucleotide-dependent dimerization of the G domains between neighboring filaments induces a movement of the G domain versus the stalk. It appears unlikely that this movement can be transmitted to the stalk of the same MxA molecule via the two flexible hinge regions. However, the identified interface between the BSE and stalk of the neighboring molecule is a prime candidate for coupling conformational changes in the G domain with an effector function in the stalk. Coupling of nucleotide hydrolysis to conformational changes in the neighboring molecule is also observed in other molecular machines, for example in triple AAA ATPases such as dynein (Carter et al., 2011). Furthermore, the identified BSE-stalk interface is important not only for the function of MxA but also for the related dynamin protein (Faelber et al., 2011).

The current MxA structure has profound implications for a better understanding of the antiviral function of MxA. First, it explains the phenotype of mutations shown previously to interfere with antiviral activity. For example, Arg633 in MxA is located in hinge 1 between stalk and BSE. Amino acid substitutions at the corresponding residue in rat Mx2 were shown to abolish antiviral activity (Johannes et al., 1997), presumably by disrupting necessary contacts between BSE and stalk. Likewise, a mutation of Glu645 to arginine in the BSE was reported to alter the antiviral specificity of MxA without affecting its GTPase activity (Zürcher et al., 1992a; Kochs et al., 2002b). According to our model, Glu645 is located in $\alpha 3^B$ and is accessible for potential interaction partners. This region has also been shown to contain a nuclear localization sequence in murine Mx1 (Zürcher et al., 1992b) that might interact with the nuclear translocation machinery.

Second, the MxA structure suggests a molecular model for MxA action. Experimental evidence points to a direct interaction of MxA with viral nucleocapsids. In negative-strand RNA viruses, they represent ribonucleoprotein complexes that consist of the viral genomic RNA associated with the viral nucleoprotein and the viral polymerase. MxA was shown to bind to the nucleoprotein N of LACV and to form intracellular MxA-N complexes (Kochs et al., 2002b), leading to depletion of N from viral replication sites (Reichelt et al., 2004). A physical interaction of MxA with the viral nucleoprotein NP was also demonstrated for influenza A viruses (Turan et al., 2004) and the closely related Thogoto virus (Kochs and Haller, 1999). Finally, interaction with NP is suggested by the fact that the viral NP determines the relative Mx sensitivities of avian versus human influenza A virus strains (Zimmermann et al., 2011). We propose that the MxA oligomeric rings represent antiviral molecular machines that oligomerize around the viral nucleocapsid structure. Conformational changes upon GTP binding and/or hydrolysis might then lead to disintegration of the infecting nucleocapsids. It is conceivable that additional host cell factors are involved and may modulate the antiviral activity and specificity (Zürcher et al., 1992b; Engelhardt et al., 2001; Wisskirchen et al., 2011). Besides negative-strand RNA viruses, Mx proteins are able to inhibit a range of additional viruses, among them double-stranded RNA viruses or some DNA viruses (Mundt, 2007; Netherton et al., 2009). In each instance, the same basic inhibitory mechanism may apply, because the Mx block generally occurs early in the viral life cycle, is affected by the same Mx-inactivating mutations, and is linked to the recruitment of the Mx GTPase to the viral replication sites. Also, human MxA was reported to inhibit the amplification of a Semliki Forest virus-based replicon in the absence of viral structural proteins (Landis et al., 1998). It will be interesting to unravel the common denominator of Mx sensitivity in these highly divergent viruses.

The present crystal structure of MxA and the identification of the oligomerization mechanism provide a molecular framework to understand the antiviral function of MxA. Importantly, the identification of the BSE-stalk interface and hinge 1 as crucial structural elements not only sheds light on the molecular mechanism of the mechano-chemical coupling during the antiviral

action of Mx GTPases but also yields functional insights into the molecular mechanisms of the related dynamins.

EXPERIMENTAL PROCEDURES

Protein Expression and Purification

Human MxA constructs including or excluding the N-terminal 32 residues (MxA or $MxA^{\Delta 1-32}$) carrying the YRGR440-443AAAA mutation in loop $L2^S$ and a deletion of amino acids 533–561 (loop $L4^S$) and the SeMet-substituted variant were prepared as described (Gao et al., 2010).

Crystallization and Structure Determination

Crystallization trials by the sitting-drop vapor-diffusion method were performed at 20°C. 1 μl of MxA or $MxA^{\Delta 1-32}$ at a concentration of 10–20 mg/ml were mixed with an equal volume of reservoir solution containing 7% PEG3350, 100 mM HEPES (pH 7.6), 80 mM NaCl, 2.5% 2-methyl-2,4-pentandiol (MPD), and 5% glycerol. Crystals appeared after 2 days and reached their final size (0.2 mm × 0.2 mm × 0.8 mm) within 5 days. Crystals of the SeMet protein (which contained the N-terminal 32 residues) were obtained in 5% PEG 3350, 100 mM HEPES (pH 7.5), 80 mM NaCl, 2% MPD, and 2% ethylene glycol. For flash-cooling of the crystals in liquid nitrogen, a cryo-solution containing 4% PEG3350, 60 mM HEPES (pH 7.6), 150 mM NaCl, 1 mM DTT, 2% MPD, 3% glycerol, and 10% PEG200 was used for native human MxA crystals and 3% PEG3350, 60 mM HEPES (pH 7.5), 150 mM $MgCl_2$, 1 mM DTT, 2% MPD, and 11% ethylene glycol was used for SeMet-substituted MxA. Native data sets for both constructs were collected from single crystals on beamline MX14.1 at BESSY and processed and scaled with the XDS program suite (Kabsch, 2010) and the Diffraction Anisotropy Server (Strong et al., 2006). The phase problem was solved by molecular replacement by Phaser (McCoy et al., 2007), with the human MxA stalk (Gao et al., 2010) and the nucleotide-free rat dynamin-1 G domain (Reubold et al., 2005) as search models. Additional electron density of the C-terminal helix of the GED and three loops not present in the search models, namely $L1^{BS}$, $L2^S$, and $L2^{BS}$, was clearly discernable (Figures S1B–S1D). Model building was done with COOT (Emsley and Cowtan, 2004). Refinement was carried out with CNS employing a deformable elastic network (DEN) (Schröder et al., 2010). A homology model of the MxA G domain was calculated based on the nucleotide-free rat G domain of dynamin with the SWISS-MODEL server (Guex and Peitsch, 1997) and was used, together with the stalk structure of human MxA, to set up DEN restraints. The G domain was less well defined in the electron density than the stalk and the BSE because it was only loosely stabilized by crystal contacts (see Figure S6). For both MxA and $MxA^{\Delta 1-32}$, electron density could be modeled from residue 45. Because of the better quality, data of $MxA^{\Delta 1-32}$ were used for the final refinement (Table 1). To verify the sequence of the low-resolution structure, a data set of a SeMet-substituted crystal was collected at peak wavelength on beamline X06SA at the Swiss Light Source (SLS). An anomalous difference Fourier map was calculated in CCP4 (CCP4, 1994) with the phases of the refined model. Eight out of nine selenium atoms in the stalk and one out of three in the G domain were used to confirm the sequence (Figure S1A). The final model has an excellent geometry at the given resolution, with 87.8% of all residues in the most favored region and 0.2% of the residues in the disallowed region of the Ramachandran plot, as determined by PROCHECK (Laskowski et al., 1993). Figures were prepared with PyMOL (http://www.pymol.org).

Right Angle Light Scattering

A coupled RALS-refractive index detector (Malvern) was connected in line to an analytical gel filtration column Superdex200 10/300 to determine absolute molecular masses of the applied proteins. Data were analyzed with the provided software. The running buffer contained 20 mM HEPES (pH 7.5), 400 mM NaCl, 2 mM $MgCl_2$, and 2 mM DTT. For each protein sample, 100 μl of a 2 mg/ml solution was applied.

Oligomerization Assay

Oligomerization assays were carried out at 2.3 mg/ml (30 μM) full-length protein in the absence and presence of 1 mM GTPγS. Samples were incubated at room temperature for 10 min in a buffer containing 20 mM HEPES (pH 7.5), 300 mM NaCl, and 2 mM $MgCl_2$. After ultracentrifugation at 200,000 × g, 25°C for 10 min, equivalent amounts of supernatant and pellet were loaded on SDS-PAGE. Results shown are representative for two independent experiments.

GTP Hydrolysis Assay

GTPase activities of human MxA and the indicated mutants were determined at 37°C in 50 mM HEPES (pH 7.5), 150 mM NaCl, 5 mM KCl, and 5 mM $MgCl_2$, with different MxA concentrations. Saturating concentrations of GTP were employed for each reaction. Reactions were initiated by the addition of protein to the final reaction solution. At different time points, reaction aliquots were 20-fold diluted in GTPase buffer and quickly transferred in liquid nitrogen. Nucleotides in the samples were separated via a reversed-phase Hypersil ODS-2 C18 column (250 × 4 mm), with 10 mM tetrabutylammonium bromide, 100 mM potassium phosphate (pH 6.5), and 7.5% acetonitrile as running buffer, where denatured proteins were adsorbed at a C18 guard column. Nucleotides were detected by absorption at 254 nm and quantified by integration of the corresponding peaks. Rates derived from a linear fit to the initial rate of the reaction (<40% GTP hydrolyzed) were plotted against the protein concentrations.

Cells and Viruses

Human embryonic kidney cells (293T) and Vero cells were maintained in Dulbecco's modified Eagle medium with 10% fetal calf serum. The original LACV strain from Reichelt et al. (2004) was used.

Influenza A Virus Minireplicon System

cDNAs of the viral polymerase subunits (PA, PB1, and PB2) and the viral nucleoprotein (NP) were derived from influenza A/Vietnam/1203/04 virus. 293T cells in 12-well plates were transfected with Nanofectin (PAA). A total of 10 ng of the three plasmids encoding the subunits of viral RNA polymerase and 100 ng for NP were cotransfected with 50 ng of plasmid pPOLI-Luc-RT carrying the firefly luciferase reporter gene as described (Zimmermann et al., 2011). To measure transfection efficiency, 25 ng of the *Renilla* luciferase-encoding plasmid pRL-SV40-R*luc* (Promega) was cotransfected. For MxA expression, 300 ng of the Mx-encoding plasmids were cotransfected. The negative control lacked the plasmid encoding NP. Cells were lysed 24 hr after transfection. Firefly and *Renilla* luciferase activities were determined with the Dual Luciferase assay (Promega).

Immunoblot Analysis

Cell lysates were analyzed by SDS-PAGE and immunoblot probed with monoclonal mouse antibody M143 directed against MxA (Flohr et al., 1999), monoclonal mouse antibody directed against FLUAV NP (Serotec), monoclonal mouse antibody against β-tubulin (Sigma), and horseradish peroxidase-conjugated secondary antibodies.

Immunofluorescence Analysis

Vero cells were prepared and stained for MxA proteins and viral antigens by indirect immunofluorescence as described previously (Reichelt et al., 2004). MxA was detected with the monoclonal mouse antibody M143, LACV N protein with a polyclonal rabbit antibody. TO-PRO-3 iodide (Invitrogen) was used for nuclear staining. Alexa Fluor 555 (Invitrogen) and Alexa Fluor 488 (Invitrogen)-conjugated donkey secondary antibodies and a Leica TCS SP II confocal microscope were used for the detection of the proteins.

ACCESSION NUMBERS

The atomic coordinates of the MxA structure have been deposited in the Protein Data Bank with accession code 3SZR.

SUPPLEMENTAL INFORMATION

Supplemental Information includes six figures and one movie and can be found with this article online at doi:10.1016/j.immuni.2011.07.012.

ACKNOWLEDGMENTS

This project was supported by grants of the Deutsche Forschungsgemeinschaft (SFB 740/TP C7 and SFB958/A12 to O.D. and Ko1579/8-1 to G.K.), by a Career Development Fellowship of The International Human Frontier Science Program Organization, and by the EMBO Young Investigator Program to O.D. We are grateful to A. Brunger for providing us with the prerelease of CNS version 1.3, the BESSY staff at beamline BL14.1 and SLS staff at beamline X06SA for help with data collection, and S. Werner, S. Paeschke, and S. Gruber for technical assistance.

Received: June 8, 2011
Revised: July 20, 2011
Accepted: July 21, 2011
Published online: September 29, 2011

REFERENCES

Accola, M.A., Huang, B., Al Masri, A., and McNiven, M.A. (2002). The antiviral dynamin family member, MxA, tubulates lipids and localizes to the smooth endoplasmic reticulum. J. Biol. Chem. *277*, 21829–21835.

Arnheiter, H., and Haller, O. (1988). Antiviral state against influenza virus neutralized by microinjection of antibodies to interferon-induced Mx proteins. EMBO J. *7*, 1315–1320.

Bian, X., Klemm, R.W., Liu, T.Y., Zhang, M., Sun, S., Sui, X., Liu, X., Rapoport, T.A., and Hu, J. (2011). Structures of the atlastin GTPase provide insight into homotypic fusion of endoplasmic reticulum membranes. Proc. Natl. Acad. Sci. USA *108*, 3976–3981.

Byrnes, L.J., and Sondermann, H. (2011). Structural basis for the nucleotide-dependent dimerization of the large G protein atlastin-1/SPG3A. Proc. Natl. Acad. Sci. USA *108*, 2216–2221.

Carter, A.P., Cho, C., Jin, L., and Vale, R.D. (2011). Crystal structure of the dynein motor domain. Science *331*, 1159–1165.

Chappie, J.S., Acharya, S., Liu, Y.W., Leonard, M., Pucadyil, T.J., and Schmid, S.L. (2009). An intramolecular signaling element that modulates dynamin function in vitro and in vivo. Mol. Biol. Cell *20*, 3561–3571.

Chappie, J.S., Acharya, S., Leonard, M., Schmid, S.L., and Dyda, F. (2010). G domain dimerization controls dynamin's assembly-stimulated GTPase activity. Nature *465*, 435–440.

CCP4 (Collaborative Computational Project, Number 4). (1994). The CCP4 suite: programs for protein crystallography. Acta Crystallogr. D Biol. Crystallogr. *50*, 760–763.

Daumke, O., Lundmark, R., Vallis, Y., Martens, S., Butler, P.J., and McMahon, H.T. (2007). Architectural and mechanistic insights into an EHD ATPase involved in membrane remodelling. Nature *449*, 923–927.

Di Paolo, C., Hefti, H.P., Meli, M., Landis, H., and Pavlovic, J. (1999). Intramolecular backfolding of the carboxyl-terminal end of MxA protein is a prerequisite for its oligomerization. J. Biol. Chem. *274*, 32071–32078.

Emsley, P., and Cowtan, K. (2004). Coot: model-building tools for molecular graphics. Acta Crystallogr. D Biol. Crystallogr. *60*, 2126–2132.

Engelhardt, O.G., Ullrich, E., Kochs, G., and Haller, O. (2001). Interferon-induced antiviral Mx1 GTPase is associated with components of the SUMO-1 system and promyelocytic leukemia protein nuclear bodies. Exp. Cell Res. *271*, 286–295.

Faelber, K., Posor, Y., Gao, S., Held, M., Roske, Y., Schulze, D., Haucke, V., Noe, F., and Daumke, O. (2011). Crystal structure of nucleotide-free dynamin. Nature, in press. Published online September 18, 2011. 10.1038/nature10369.

Flohr, F., Schneider-Schaulies, S., Haller, O., and Kochs, G. (1999). The central interactive region of human MxA GTPase is involved in GTPase activation and interaction with viral target structures. FEBS Lett. *463*, 24–28.

Gao, S., von der Malsburg, A., Paeschke, S., Behlke, J., Haller, O., Kochs, G., and Daumke, O. (2010). Structural basis of oligomerization in the stalk region of dynamin-like MxA. Nature *465*, 502–506.

Guex, N., and Peitsch, M.C. (1997). SWISS-MODEL and the Swiss-PdbViewer: an environment for comparative protein modeling. Electrophoresis *18*, 2714–2723.

Haller, O., and Kochs, G. (2011). Human MxA protein: an interferon-induced dynamin-like GTPase with broad antiviral activity. J. Interferon Cytokine Res. *31*, 79–87.

Holzinger, D., Jorns, C., Stertz, S., Boisson-Dupuis, S., Thimme, R., Weidmann, M., Casanova, J.L., Haller, O., and Kochs, G. (2007). Induction of MxA gene expression by influenza A virus requires type I or type III interferon signaling. J. Virol. *81*, 7776–7785.

Hunn, J.P., Feng, C.G., Sher, A., and Howard, J.C. (2011). The immunity-related GTPases in mammals: a fast-evolving cell-autonomous resistance system against intracellular pathogens. Mamm. Genome *22*, 43–54.

Johannes, L., Kambadur, R., Lee-Hellmich, H., Hodgkinson, C.A., Arnheiter, H., and Meier, E. (1997). Antiviral determinants of rat Mx GTPases map to the carboxy-terminal half. J. Virol. *71*, 9792–9795.

Kabsch, W. (2010). XDS. Acta Crystallogr. D Biol. Crystallogr. *66*, 125–132.

Kenniston, J.A., and Lemmon, M.A. (2010). Dynamin GTPase regulation is altered by PH domain mutations found in centronuclear myopathy patients. EMBO J. *29*, 3054–3067.

Kochs, G., and Haller, O. (1999). GTP-bound human MxA protein interacts with the nucleocapsids of Thogoto virus (Orthomyxoviridae). J. Biol. Chem. *274*, 4370–4376.

Kochs, G., Haener, M., Aebi, U., and Haller, O. (2002a). Self-assembly of human MxA GTPase into highly ordered dynamin-like oligomers. J. Biol. Chem. *277*, 14172–14176.

Kochs, G., Janzen, C., Hohenberg, H., and Haller, O. (2002b). Antivirally active MxA protein sequesters La Crosse virus nucleocapsid protein into perinuclear complexes. Proc. Natl. Acad. Sci. USA *99*, 3153–3158.

Landis, H., Simon-Jödicke, A., Klöti, A., Di Paolo, C., Schnorr, J.J., Schneider-Schaulies, S., Hefti, H.P., and Pavlovic, J. (1998). Human MxA protein confers resistance to Semliki Forest virus and inhibits the amplification of a Semliki Forest virus-based replicon in the absence of viral structural proteins. J. Virol. *72*, 1516–1522.

Laskowski, R.A., Macarthur, M.W., Moss, D.S., and Thornton, J.M. (1993). Procheck—a program to check the stereochemical quality of protein structures. J. Appl. Cryst. *26*, 283–291.

Lindenmann, J. (1964). Inheritance of resistance to influenza virus in mice. Proc. Soc. Exp. Biol. Med. *116*, 506–509.

Low, H.H., and Löwe, J. (2010). Dynamin architecture—from monomer to polymer. Curr. Opin. Struct. Biol. *20*, 791–798.

McCoy, A.J., Grosse-Kunstleve, R.W., Adams, P.D., Winn, M.D., Storoni, L.C., and Read, R.J. (2007). Phaser crystallographic software. J. Appl. Cryst. *40*, 658–674.

Mears, J.A., Ray, P., and Hinshaw, J.E. (2007). A corkscrew model for dynamin constriction. Structure *15*, 1190–1202.

Melén, K., Ronni, T., Broni, B., Krug, R.M., von Bonsdorff, C.H., and Julkunen, I. (1992). Interferon-induced Mx proteins form oligomers and contain a putative leucine zipper. J. Biol. Chem. *267*, 25898–25907.

Mibayashi, M., Nakad, K., and Nagata, K. (2002). Promoted cell death of cells expressing human MxA by influenza virus infection. Microbiol. Immunol. *46*, 29–36.

Miller, S., and Krijnse-Locker, J. (2008). Modification of intracellular membrane structures for virus replication. Nat. Rev. Microbiol. *6*, 363–374.

Mundt, E. (2007). Human MxA protein confers resistance to double-stranded RNA viruses of two virus families. J. Gen. Virol. *88*, 1319–1323.

Mushinski, J.F., Nguyen, P., Stevens, L.M., Khanna, C., Lee, S., Chung, E.J., Lee, M.J., Kim, Y.S., Linehan, W.M., Horisberger, M.A., and Trepel, J.B. (2009). Inhibition of tumor cell motility by the interferon-inducible GTPase MxA. J. Biol. Chem. *284*, 15206–15214.

Netherton, C.L., Simpson, J., Haller, O., Wileman, T.E., Takamatsu, H.H., Monaghan, P., and Taylor, G. (2009). Inhibition of a large double-stranded DNA virus by MxA protein. J. Virol. *83*, 2310–2320.

Pavlovic, J., Haller, O., and Staeheli, P. (1992). Human and mouse Mx proteins inhibit different steps of the influenza virus multiplication cycle. J. Virol. *66*, 2564–2569.

Pitossi, F., Blank, A., Schröder, A., Schwarz, A., Hüssi, P., Schwemmle, M., Pavlovic, J., and Staeheli, P. (1993). A functional GTP-binding motif is necessary for antiviral activity of Mx proteins. J. Virol. *67*, 6726–6732.

Prakash, B., Praefcke, G.J., Renault, L., Wittinghofer, A., and Herrmann, C. (2000). Structure of human guanylate-binding protein 1 representing a unique class of GTP-binding proteins. Nature *403*, 567–571.

Ramachandran, R., Surka, M., Chappie, J.S., Fowler, D.M., Foss, T.R., Song, B.D., and Schmid, S.L. (2007). The dynamin middle domain is critical for tetramerization and higher-order self-assembly. EMBO J. *26*, 559–566.

Reichelt, M., Stertz, S., Krijnse-Locker, J., Haller, O., and Kochs, G. (2004). Missorting of LaCrosse virus nucleocapsid protein by the interferon-induced MxA GTPase involves smooth ER membranes. Traffic *5*, 772–784.

Reubold, T.F., Eschenburg, S., Becker, A., Leonard, M., Schmid, S.L., Vallee, R.B., Kull, F.J., and Manstein, D.J. (2005). Crystal structure of the GTPase domain of rat dynamin 1. Proc. Natl. Acad. Sci. USA *102*, 13093–13098.

Schröder, G.F., Levitt, M., and Brunger, A.T. (2010). Super-resolution biomolecular crystallography with low-resolution data. Nature *464*, 1218–1222.

Schwemmle, M., Richter, M.F., Herrmann, C., Nassar, N., and Staeheli, P. (1995). Unexpected structural requirements for GTPase activity of the interferon-induced MxA protein. J. Biol. Chem. *270*, 13518–13523.

Sever, S., Muhlberg, A.B., and Schmid, S.L. (1999). Impairment of dynamin's GAP domain stimulates receptor-mediated endocytosis. Nature *398*, 481–486.

Speiser, D.E., Zürcher, T., Ramseier, H., Hengartner, H., Staeheli, P., Haller, O., and Zinkernagel, R.M. (1990). Nuclear myxovirus-resistance protein Mx is a minor histocompatibility antigen. Proc. Natl. Acad. Sci. USA *87*, 2021–2025.

Staeheli, P., Haller, O., Boll, W., Lindenmann, J., and Weissmann, C. (1986). Mx protein: constitutive expression in 3T3 cells transformed with cloned Mx cDNA confers selective resistance to influenza virus. Cell *44*, 147–158.

Staeheli, P., Grob, R., Meier, E., Sutcliffe, J.G., and Haller, O. (1988). Influenza virus-susceptible mice carry Mx genes with a large deletion or a nonsense mutation. Mol. Cell. Biol. *8*, 4518–4523.

Stertz, S., Reichelt, M., Krijnse-Locker, J., Mackenzie, J., Simpson, J.C., Haller, O., and Kochs, G. (2006). Interferon-induced, antiviral human MxA protein localizes to a distinct subcompartment of the smooth endoplasmic reticulum. J. Interferon Cytokine Res. *26*, 650–660.

Strong, M., Sawaya, M.R., Wang, S., Phillips, M., Cascio, D., and Eisenberg, D. (2006). Toward the structural genomics of complexes: crystal structure of a PE/PPE protein complex from Mycobacterium tuberculosis. Proc. Natl. Acad. Sci. USA *103*, 8060–8065.

Turan, K., Mibayashi, M., Sugiyama, K., Saito, S., Numajiri, A., and Nagata, K. (2004). Nuclear MxA proteins form a complex with influenza virus NP and inhibit the transcription of the engineered influenza virus genome. Nucleic Acids Res. *32*, 643–652.

von der Malsburg, A., Abutbul, I., Haller, O., Kochs, G., and Danino, D. (2011). The stalk domain of the dynamin-like MxA GTPase mediates membrane binding and liposome tubulation via the unstructured l4 loop. J. Biol. Chem., in press. Published online September 7, 2011. 10.1074/jbc.M111.249037.

Wisskirchen, C., Ludersdorfer, T.H., Mueller, D.A., Moritz, E., and Pavlovic, J. (2011). The interferon induced antiviral protein MxA interacts with the cellular RNA Helicases UAP56 and URH49. J. Biol. Chem., in press. Published online August 22, 2011. 10.1074/jbc.M111.251843.

Wolf, D., and Goff, S.P. (2008). Host restriction factors blocking retroviral replication. Annu. Rev. Genet. *42*, 143–163.

Zimmermann, P., Mänz, B., Haller, O., Schwemmle, M., and Kochs, G. (2011). The viral nucleoprotein determines Mx sensitivity of influenza A viruses. J. Virol. *85*, 8133–8140.

Zürcher, T., Pavlovic, J., and Staeheli, P. (1992a). Mechanism of human MxA protein action: variants with changed antiviral properties. EMBO J. *11*, 1657–1661.

Zürcher, T., Pavlovic, J., and Staeheli, P. (1992b). Nuclear localization of mouse Mx1 protein is necessary for inhibition of influenza virus. J. Virol. *66*, 5059–5066.